Dynamic interaction between suspended particles and defects in a nematic liquid crystal

S. Grollau, N. L. Abbott, and J. J. de Pablo
Department of Chemical Engineering, University of Wisconsin, 1415 Engineering Drive, Madison, Wisconsin 53706
(Received 21 November 2002; published 13 May 2003)

Insertion of spherical particles into a uniform nematic liquid crystal gives rise to the formation of topological defects. In the present work, we investigate how a spherical particle accompanied by its topological defects interacts with neighboring disclination lines. We perform two- and three-dimensional dynamic simulations to analyze the effect of a particle on the annihilation process of two disclination lines. The dynamics of the liquid crystal is described by a time-dependent evolution equation on the symmetric traceless order parameter that includes some of the salient features of liquid crystalline materials: excluded volume effects, or equivalently, short-range order elasticity and long-range order elasticity. At the surface of the particle, the liquid crystal is assumed to exhibit strong homeotropic anchoring. The particle is located between two disclination lines of topological charges $+1/2$ and $-1/2$. Two-dimensional simulations indicate that the topological defects bound to the particle mediate an interaction between the two disclination lines which increases the attraction between them. This result is confirmed by three-dimensional simulations that provide a complete description of the director field and of the order parameter around the particle. These simulations indicate that a spherical particle between two disclination lines can be surrounded by a Saturn ring, and suggest that the dynamic behavior of disclination lines could be used to report the structure of a defect around the particle.

DOI: 10.1103/PhysRevE.67.051703 PACS number(s): 61.30.Jf, 77.84.Nh, 61.30.Cz, 42.79.Kr

I. INTRODUCTION

Colloidal systems and emulsions in anisotropic host fluids such as liquid crystals are of considerable interest in a wide variety of applications. Past experimental studies have reported that the introduction of isotropic liquid microdroplets into uniformly aligned nematic liquid crystals is accompanied by the formation of topological defects around the droplets [1]. One important characteristic of such systems is the orientation of the molecules at the surface of the particle (referred to as anchoring conditions), which can yield various nontrivial configurations of the nematic liquid crystal.

The design of liquid-crystal based devices requires control of the orientation of the molecules at the different surfaces present in the system. For a water droplet in a liquid crystal, the anchoring conditions can be controlled by using various amphiphilic compounds adsorbed at the droplet-liquid crystal interface. At solid surfaces, the control of the orientation of the molecules can be achieved through various treatments of the substrate, such as mechanical rubbing [2] or the chemisorption of alkanethiols [3]. In this latter approach, the control on the orientation of the molecules as well as the strength of the anchoring is achieved through the use of self-assembled monolayers of different compositions. This technique has been used in different contexts and, in particular, to observe topological defects around solid particles in a confined geometry [4]. It has also been used in applications of liquid crystals to optical amplification of ligand-receptor binding [5], where the ligand-mediated binding of proteins at solid surfaces distorts the uniform nematic order by creating topological defects or disclination lines. This destruction of the uniform nematic order gives rise to an optical signature of the presence of proteins bound at the solid surfaces, thereby providing a basis for development of sensors.

The possibility that a particle with homeotropic anchoring might be surrounded by a Saturn ring disclination line was first proposed by theoretical studies [6,7] and later confirmed in experimental observations [4,8]. An alternative possibility is that a particle can be accompanied by a point defect (hyperbolic hedgehog configuration) [1,9]. The stability of the corresponding director configurations depends on many factors, including the size of the particle, the application of an external field [10], the strength of the anchoring [11], and the presence of confining surfaces in the system [12].

The nonlinearity of the Euler-Lagrange equations that describe the elastic deformations of the nematic liquid crystal makes these problems nontrivial. Some of the available theoretical studies have been restricted to the linear regime in the weak anchoring limit [13,14] or have been based on ansatz functions [6,7,9]. Numerical simulations have become more common in recent years. Within the director description, the configuration of nematogens around a spherical particle has been studied through the use of Monte-Carlo simulations [11], where the analysis was focused on the effects of anchoring strength. Several authors have investigated the effect of the particle size and of the presence of confining surfaces through numerical minimization of the Frank free energy [10,12]. The director configuration around a particle has also been analyzed with molecular dynamics [15,16]. More recently, a Monte-Carlo method has been developed to study the interaction between a particle and a hard wall [17]. In this last study, a method based on the combination of canonical expanded ensemble simulations with a density-of-states formalism was proposed to obtain the potential of mean force between the particle and the wall.

Most of the previous studies based on the minimization of the elastic free energy have been performed within the director description. One important limitation of the director description is the restriction of the formalism to an uniaxial order parameter of constant magnitude. The director description, however, is not appropriate for study of the region in the neighborhood of the core defect, where it is known that

the magnitude of the order parameter exhibits a steep gradient [18]. To obtain reliable estimates of the free energy within the director description, one can introduce, for instance, approximate energetic contributions in the neighborhood of the defect [10,12]. A better approach towards description of structure of the core defect (as well as its dynamic behavior) relies on the second-rank tensor order parameter **Q**. Recently, within this latter formalism, careful analyses have been performed to study the dynamics of two disclination lines in an annihilation process and the back flow effects (see Ref. [19], and references herein). Within the tensor order parameter formalism, a numerical analysis based on an adaptive grid has been performed to study the director configuration around a spherical particle in two dimensions [20]. In this work, we use the tensor formalism to examine how the dynamics of disclination lines is affected by the presence of a particle accompanied by its topological defects. We view this study as a first step towards understanding how topological defects arise and evolve in many-particle systems when liquid crystals are used in sensors [5].

The paper is organized as follows. In Sec. II, we introduce the model. In Sec. III, we present and discuss the results. We first study the insertion of a single particle in a nematic. The effect of the size of the particle on the location of the defects and the breakdown of the continuum limit is investigated. The dynamic behavior of two disclination lines of opposite charges is then investigated. we use two- and three-dimensional simulations to analyze how the presence of a particle with its topological defects affects and distorts the disclination lines.

II. THE MODEL

On the macroscopic level, nematics with uniaxial symmetry around a given direction can be described by the director **n**. In the director description [21], the nematic order parameter is assumed to be constant. The defects that appear in liquid crystalline materials are characterized by a steep gradient in the magnitude of the nematic order parameter, reflecting that locally the liquid crystal ''melts,'' and also by a strong biaxiality within the core region [18]. The director description is thus not appropriate to investigate the structure of core defects and their dynamic behavior. To describe the dynamic behavior of topological defects, one needs to introduce more microscopic degrees of freedom.

At the microscopic level, nematogens can be characterized by a nonisotropic distribution function $\psi(\mathbf{u})$, which measures the probability that a molecule is oriented in the direction **u**. The simplest quantity representing the anisotropy is the symmetric traceless tensor order parameter

$$\mathbf{Q}_{\alpha\beta}=\left\langle u_\alpha u_\beta-\frac{1}{3}\delta_{\alpha\beta}\right\rangle, \tag{1}$$

where the brackets $\langle A\rangle=\int A\psi(\mathbf{u})d\mathbf{u}_s$ denote an average over all possible orientations on the unit sphere. In the present work, we are interested in macroscopic samples for which the order parameter varies with position. In this description, the tensor $\mathbf{Q}(\mathbf{r})$ defines a coarse-grained order parameter that represents the local average, Eq. (1), at point **r**. (It is implicitly assumed in this coarse-grained description that the local average corresponds to one monodomain characterized by a probability distribution function $\psi(u)$ that depends on the spacial position **r**.) In what follows, Greek indices are used to represent Cartesian directions, and the usual sum over repeated indices is assumed.

The equilibrium properties of the liquid crystal are described by the Landau-De Gennes free energy [21]. This comprises a contribution describing the long-range elastic forces in the nematic phase

$$\mathcal{F}_e=\int d\mathbf{r}\,\frac{L_1}{2}(\partial_\alpha Q_{\beta\gamma})^2, \tag{2}$$

where L_1 is a material-specific elastic constant and, second, a short-range elastic contribution of the form

$$\mathcal{F}_s=\int d\mathbf{r}\left\{\frac{A}{2}\left(1-\frac{U}{3}\right)Q_{\alpha\beta}Q_{\alpha\beta}-\frac{AU}{3}Q_{\nu\gamma}Q_{\nu\alpha}Q_{\alpha\gamma}+\frac{AU}{4}(Q_{\alpha\beta}Q_{\alpha\beta})^2\right\}, \tag{3}$$

which is representative of the excluded volume effects responsible for the first-order transition from the isotropic to the nematic phase. In this model, the first-order transition occurs at a magnitude of the nematic potential $U=2.7$. (Starting from a kinetic theory, one can relate the nematic potential U to the number of molecules per unit of volume, when the excluded volume effects are treated through the Onsager potential. For a detailed discussion, see Ref. [22].) The relative magnitude between the two contributions, Eq. (2) and Eq. (3), depends on the liquid crystal of interest. For polymeric liquid crystals, short-range interactions are dominant, whereas long-range interactions are dominant for low molecular weight liquid crystals. The parameter A is introduced to control the relative magnitude of the two contributions. Given the set of phenomenological parameters that arise in this theory, it is convenient to introduce the quantity $\xi=\sqrt{18L_1/AU}$ as a characteristic length scale for the order parameter changes.

In the absence of flow, the time evolution equation for **Q** is obtained from the molecular field **H** that provides the driving motion responsible for the relaxation of the order parameter towards the minimum of the free energy

$$\frac{\partial\mathbf{Q}}{\partial t}=\Gamma\mathbf{H}, \tag{4}$$

where Γ is the collective rotational diffusion constant. The molecular field is given by

$$\mathbf{H}=-\frac{\delta\mathcal{F}}{\delta\mathbf{Q}}+\frac{\mathbf{I}}{3}\mathrm{Tr}\,\frac{\delta\mathcal{F}}{\delta\mathbf{Q}}, \tag{5}$$

where $\mathcal{F}=\mathcal{F}_s+\mathcal{F}_e$ denotes the total free energy, **I** is the identity operator, and the last term corresponds to the minimization of the free energy keeping the order parameter **Q** trace-

less. From Eqs. (2)–(5), the equation of motion for the components of the tensor order parameter is given by

$$\frac{\partial Q_{\alpha\beta}}{\partial t} = -\frac{6D^{\star}}{\left(1-\frac{3}{2}Q_{\mu\nu}Q_{\mu\nu}\right)^2}\left\{A\left(1-\frac{U}{3}\right)Q_{\alpha\beta} - AU\left(Q_{\alpha\nu}Q_{\nu\beta}-\frac{\delta_{\alpha\beta}}{3}Q_{\nu\rho}Q_{\nu\rho}\right)+AUQ_{\alpha\beta}(Q_{\nu\rho}Q_{\nu\rho}) - L_1\partial_{\rho}^2 Q_{\alpha\beta}\right\}. \tag{6}$$

The above equation is the time evolution equation for the order parameter and corresponds to a particular case of the Beris-Edwards formulation [23], where Γ is related to the rotational diffusivity coefficient $D^{\star}$ through the relation $\Gamma = 6D^{\star}/(1-\frac{3}{2}Q_{\mu\nu}Q_{\mu\nu})^2$. The domain of validity of Eq. (6) is not restricted to the neighborhood of the first-order phase transition, but it also extends into the nematic phase at high values of the nematic potential U (see the discussion in Ref. [22]).

In the most general situation, the diagonalization of the tensor order parameter has the form

$$\mathbf{Q}=\begin{pmatrix} \frac{2S}{3} & 0 & 0 \\ 0 & \frac{\eta-S}{3} & 0 \\ 0 & 0 & -\frac{\eta+S}{3} \end{pmatrix}, \tag{7}$$

where S denotes the nematic scalar order parameter and η denotes the biaxiality. The eigenvector associated with the highest eigenvalue $2S/3$ corresponds to the generalization of the director **n**. At bounding surfaces, we assume that **Q** is uniaxial and has the form

$$\mathbf{Q}=S^{eq}\left(\mathbf{nn}-\frac{1}{3}\mathbf{I}\right), \tag{8}$$

where **n** is the director at the surface and S^{eq} is the equilibrium nematic order parameter given in the Doi theory [22] by

$$S^{eq}=\frac{1}{4}+\frac{3}{4}\sqrt{1-\frac{8}{3U}}. \tag{9}$$

In the uniaxial limit, the material specific elastic constant L_1 is related to the splay K_{11}, bend K_{22}, and twist K_{33} constants through the relations [23] $L_1=K_{11}/S^2=K_{22}/S^2=K_{33}/S^2$, which correspond to the one-constant approximation. Our calculations are performed with a set of parameters that are representative of a low molecular weight liquid crystal such as pentylcyanobiphenyl (5CB) (see Ref. [24] for the simulation parameters).

An Euler scheme is used to solve Eq. (6). Derivatives are evaluated by finite difference methods on a regular grid. The insertion of a particle is implemented automatically in the numerical procedure, where the grid is defined in the entire area of interest except in the region inside the particle. At the surface of the particle, we consider the case of strong homeotropic anchoring where the equilibrium value of the order parameter is given by Eq. (9). We have used several mesh divisions for the spatial resolution of the grid and also several time steps to verify the stability of the numerical solution (see Ref. [25] for the parameters of the grid). We have performed the numerical integration on the six components of **Q**. This allows us to verify that, at each time step, the traceless condition $Q_{xx}+Q_{yy}+Q_{zz}=0$ is satisfied.

III. RESULTS AND DISCUSSION

A. One particle in a nematic liquid crystal in two dimensions: Binding of its topological defects and breakdown of the continuum limit

As mentioned in the Introduction, determining the director configuration around a spherical particle immersed in a nematic liquid crystal has been the subject of numerous studies. Most of the studies devoted to this problem have been conducted in the framework of the continuum theory; the tensor order parameter formalism has only been used rarely in this context [20].

As a first step, we consider the insertion of one spherical particle into a nematic liquid crystal. We focus our attention on the case of strong homeotropic anchoring at the surface of a particle. (The effects of varying the strength of the anchoring are not discussed here. Readers interested in the effects of strength anchoring within the director formalism are referred to the literature [6,7,11].) The initial configuration consists of a spherical particle in a uniform nematic liquid crystal. Since the particle promotes strong homeotropic anchoring, we observe that two defects of topological charge $-1/2$ are created on each side of the particle during a dynamic simulation. These two defects are first created in the neighborhood of the particle and are then repelled from the surface of the particle until they reach an equilibrium position. At equilibrium, and due to the cylindrical symmetry of the system, the corresponding director configuration is that of a particle surrounded by a Saturn ring disclination line (2D simulations miss the curvature of the line tension of disclination loops). For a particle with strong homeotropic anchoring, it is known that two defect configurations are possible: Saturn rings and hyperbolic hedgehog point defects. As indicated in Ref. [20], a director configuration with a dipolar defect (topological charge $q=-1$) is unstable and changes into a configuration with a pair of defects with topological charges $q=-1/2$. Starting a dynamic simulation from a configuration that contains a defect of topological charge -1 leads indeed to the splitting of the point defect into a defect pair of topological charge $-1/2$. For this reason, two-dimensional dynamic simulations within the tensor order parameter formalism yield a particle accompanied by two defects of charge $-1/2$. In previous numerical analyses based on the minimization of the Frank free energy [10,12,26,27], the study of the hyperbolic hedgehog configuration was only possible through an artificial numerical ''pinning'' that

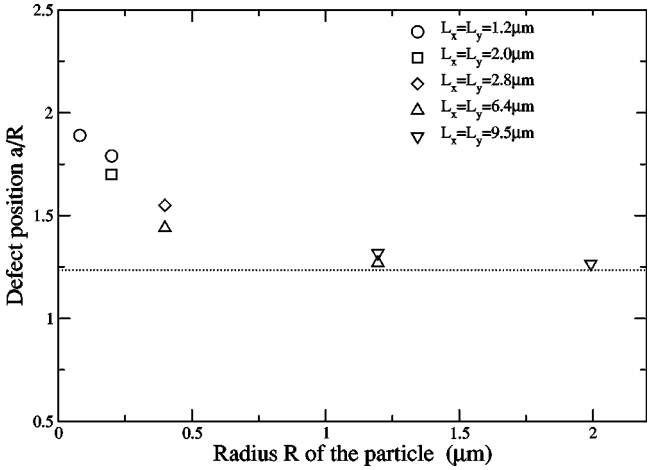

FIG. 1. Location of the defect a/R for various radii R of the particle: breakdown of the continuum limit for small particles. The dotted line represents the continuum limit Eq. (10) obtained using an electrostatic analogy [20].

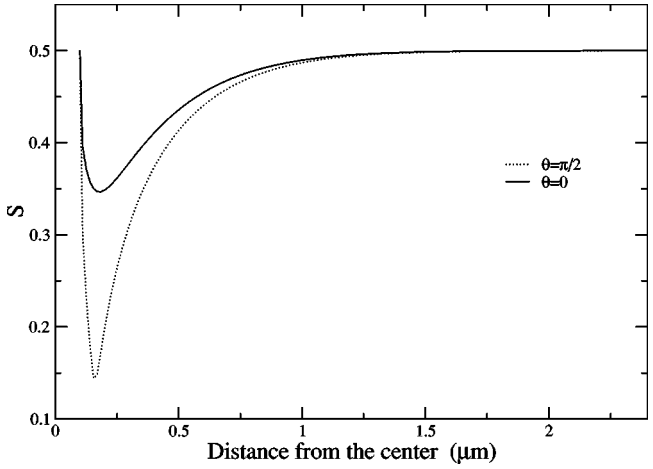

FIG. 2. Nematic scalar order parameter S around a spherical particle in the equatorial plane ($\theta=\pi/2$) and at the pole ($\theta=0$).

avoids the splitting of the point defect. This numerical pinning, which is probably due to the lack of microscopic degrees of freedom in the director description, makes the hyperbolic hedgehog configuration artificially stable in two-dimensional calculations based on the Frank free energy minimizations.

We have analyzed the equilibrium location of the two defects of charge $-1/2$ as a function of particle size. Figure 1 shows the distance a between the center of the particle and the defect position for various radii R of the particle. In the numerical procedure, the defect position is obtained by looking for the minimum value in the nematic scalar order parameter S. We have performed simulations for several sizes of the system to verify that there are no finite-size effects. (The lengths of the box are denoted by L_x and L_y.) When the size of the particle is large (see the data for $R=1.2$ μm and $R=2.0$ μm), we observe that the numerical data are in agreement with the continuum limit [20], namely:

$$a=(7/3)^{1/4}R\approx 1.236R. \tag{10}$$

Equation (10) is obtained using an electrostatic analogy. As discussed in Ref. [20], this expression should be valid when the spatial extension of the core defect is small compared to the size of the particle. Equation (10) defines the small-defect limit and should be valid for large particles or, more precisely, when the continuum formalism is appropriate to describe the director configuration around the particle. In our simulations, we observe that the small-defect limit is satisfied when the radius R of the particle is larger than ξ, the characteristic length scale for changes in the scalar order parameter ($\xi=0.7$ μm). For particles whose radii are smaller than 1 μm, we observe that the small-defect limit is not satisfied. The defects are repelled from the particle at a distance a where the ratio a/R is larger than 1.236. For instance, for a particle of radius $R=0.2$ μm, we find that the defect is located at $a\approx(0.35\pm 0.01)$ μm, giving a ratio $a/R=1.75$. In the remainder of this work, all simulations are performed with a particle of radius $R=0.2$ μm, which is commensurate with common viruses. (All lengths are given in micrometers. When one works with dimensionless quantities, the value $R=0.2$ μm corresponds to a particle of radius $R=0.5$, and this has to be compared with $\xi=1.8$.)

Figures 2 and 3 show the nematic scalar order parameter S and the biaxiality η, respectively, at equilibrium. In the equatorial plane (the plane that contains the two defects, and referred to $\theta=\pi/2$ on Figs. 2 and 3), we observe a steep gradient in the magnitude of the nematic order parameter. The core defect is characterized by a nematic order parameter that tends to zero, indicating that locally the liquid crystal ''melts,'' and also by a strong biaxiality. One might also note that at the pole (referred to $\theta=0$), the magnitude of the order parameter as well as the magnitude of the biaxiality differ from their equilibrium value in the uniaxial nematic phase, even though the director configuration does not exhibit any discontinuities at the pole. The reason for this comes from the small size of the particle that is considered here. For this submicrometer particle $R\lesssim\xi$, the spatial extension of the defect is indeed comparable to the size of the

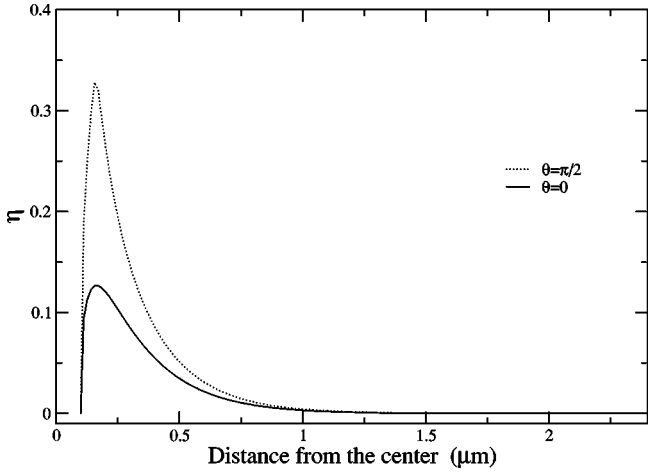

FIG. 3. Biaxiality η around a spherical particle in the equatorial plane ($\theta=\pi/2$) and at the pole ($\theta=0$).

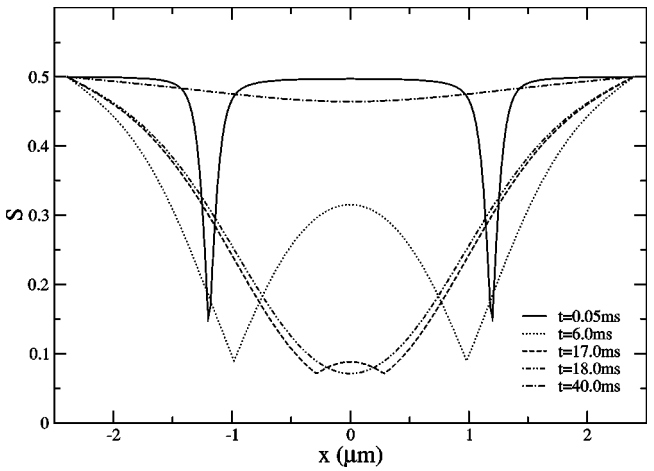

FIG. 4. Dynamic relaxation of the nematic scalar order parameter S during the annihilation of two disclination lines ($L_x = 4.8\ \mu$m).

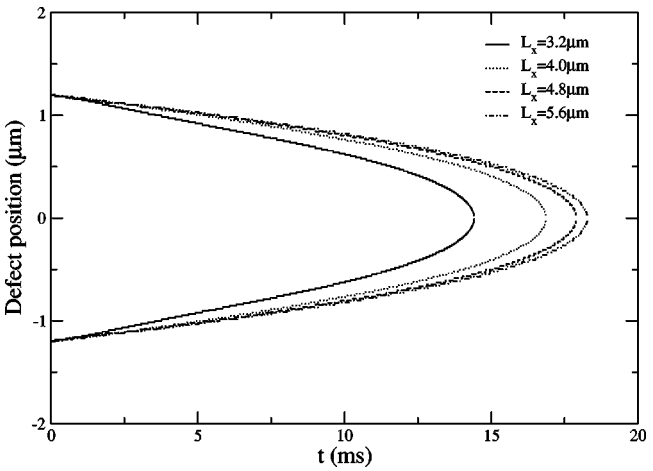

FIG. 5. Defect positions during the annihilation of two disclination lines; the positions correspond to the two coordinates x of the two disclination lines. The hard walls are separated by the distances $L_x = 3.2$, 4.0, 4.8, and 5.6 μm and are located at $x_{walls} = \pm 1.6$, ± 2.0, ± 2.4, and $\pm 2.8\ \mu$m, respectively.

particle. The core defect located in the equatorial plane of the particle influences thus the structure of the nematic even at the poles, leading to the decrease in the scalar parameter and a nonzero biaxiality at the poles of the particle.

B. Annihilation of two disclination lines in two dimensions: Effect of confining surfaces

The annihilation of two disclination lines is first examined in the absence of any particles. Simulations are started from an initial configuration where the tensor order parameter is given by Eqs. (8) and (9), and the director profile $(n_x, n_y) = (\cos\phi, \sin\phi)$ is given by the superposition of two disclination lines of opposite charge:

$$\phi = -\frac{1}{2}\tan^{-1}\left(\frac{y-y_-}{x-x_-}\right) + \frac{1}{2}\tan^{-1}\left(\frac{y-y_+}{x-x_+}\right). \qquad (11)$$

The coordinates (x_-, y_-) and (x_+, y_+) correspond to the location of the two $-1/2$ and $+1/2$ disclination lines, respectively. In our simulations, the disclination lines are separated by a distance $d_x = 2.8\ \mu$m and are located at the same vertical coordinate y, in the middle of the cell. We have analyzed the relaxation dynamics of the annihilation process when the disclination lines are located between two confining hard walls separated by a distance L_x (the two hard walls are located at the extremities of the cell, x_{min} and x_{max}). Free boundary conditions are imposed at the top and at the bottom of the cell. The relaxation dynamics of the scalar order parameter S and the effect of the confining surfaces are represented in Figs. 4 and 5, respectively. In the initial configuration, the nematic order parameter S is homogeneous, with $S_{eq} = 0.5$. As indicated in Fig. 4, at the beginning of the simulation the two defects are characterized by a strong decrease in the magnitude of S. As the disclination lines move, the two minima in S get closer to each other and collapse at the time of annihilation, between $t = 17$ ms and $t = 18$ ms. After the annihilation, there is a single minimum in S that tends to its equilibrium value (see data at $t = 40$ ms). The effects of confining surfaces are represented in Figure 5. When hard walls are separated by a distance larger than $L_x = 5.6\ \mu$m, the time for annihilation is constant and equal to $t \approx 18.3$ ms. This corresponds to the annihilation of two disclination lines in the bulk limit, when bounding surfaces do not influence the annihilation. As the hard walls get closer to the disclination lines, the time for annihilation becomes shorter. The two disclination lines are indeed repelled by the presence of the hard walls. The repulsion created by the walls does not depend on the charges of the disclination lines [21] and the defects move according to symmetric dynamical trajectories. As pointed out in previous calculations devoted to the study of the annihilation process, a dynamic simulation that includes the backflow effects would not necessarily lead to symmetric dynamical trajectories (see the recent study [19]). In the following section, the length of the box is fixed at $L_x = 4.8\ \mu$m.

C. Interaction between one particle and two disclination lines in two and three dimensions

We now consider how the presence of a particle influences the annihilation of two disclination lines. We have first performed two-dimensional simulations where a spherical particle is located in the middle of the two lines. As in the preceding section, the initial configuration is given by the director profile, Eq. (11). A particle with strong homeotropic anchoring is inserted between the two lines. The radius of the particle is fixed at $R = 0.2\ \mu$m, and the two disclination lines are separated by a distance $d_x = 2.8\ \mu$m. Figure 6 shows the director configuration at four different time steps. These ''optical pictures'' are obtained by assigning a color that is proportional to $(n_x n_y)^2$. This is representative of the intensity of the light transmitted in a direction perpendicular to the cell, when two crossed polarizers are aligned in the horizontal (or x) and vertical (or y) directions. In this optical picture, a defect of topological charges $\pm 1/2$ is characterized by two bright brushes (see Fig. 6). The schemes in Fig. 7 represent

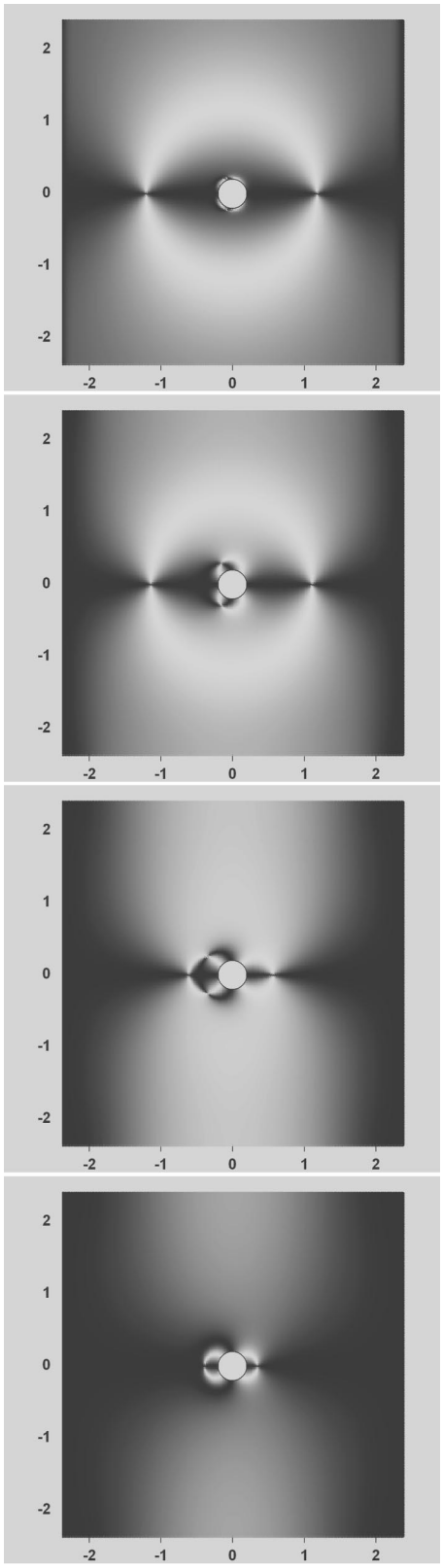

FIG. 6. Optical picture for the annihilation of two disclination lines, with a particle located in the middle of the cell: from top to bottom, the snapshots are taken at $t=0.05$, 2, 10, and 22 ms. (The lengths are given in micrometers, and $L_x=L_y=4.8$ μm.)

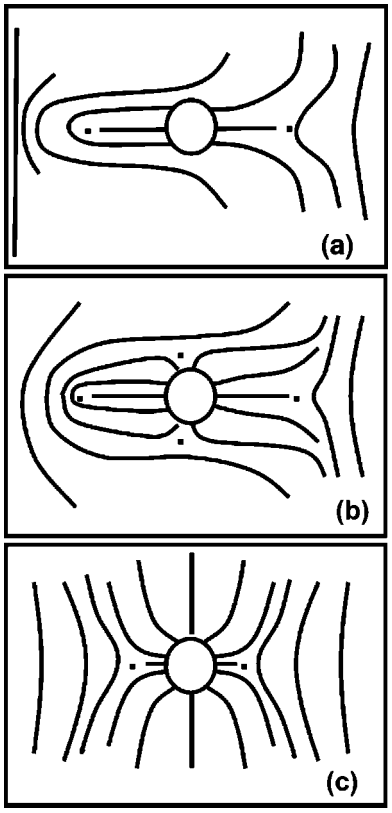

FIG. 7. Illustrative schemes representing the director profile for the annihilation of two disclination lines, with a particle located in the middle of the cell: initial configuration (a), intermediate configuration with two defects of charge $-1/2$ near the particle (b), and equilibrium configuration after annihilation (c).

the corresponding director profile for the initial configuration, an intermediate configuration with the two defects bound to the particle, and the equilibrium configuration after the annihilation. In the initial steps of the dynamic simulations, the two topological defects that are created by the particle appear at a position that is shifted in the direction of the disclination line of charge $+1/2$. When the two disclination lines are far away from the particle (see the optical picture at $t=0.05$ ms and $t=2$ ms), the director in the neighborhood of the particle is quasiuniform along the x direction and the defects are located on the top and bottom of the particle. However, they are slightly shifted in the direction of the $+1/2$ disclination line due to the attractive force between the defects of opposite charges [21]. As the disclination lines move towards the particle during the annihilation process, the defects of the particle rotate around the particle in the direction of the $+1/2$ disclination line (see the optical picture at $t=10$ ms). At a certain point, the $+1/2$ disclination line collapses with the two defects of topological charge $-1/2$. This occurs at time $t\approx 12$ ms, and it gives rise to a new configuration where there is a single topological defect of charge $-1/2$. This new defect, as well as the $-1/2$ disclination line on the right side of the particle, reach a final equilibrium location. The final configuration therefore consists of a particle with two defects of charge $-1/2$ (or equivalently, the Saturn ring configuration in two dimensions; see the optical picture at $t=22$ ms).

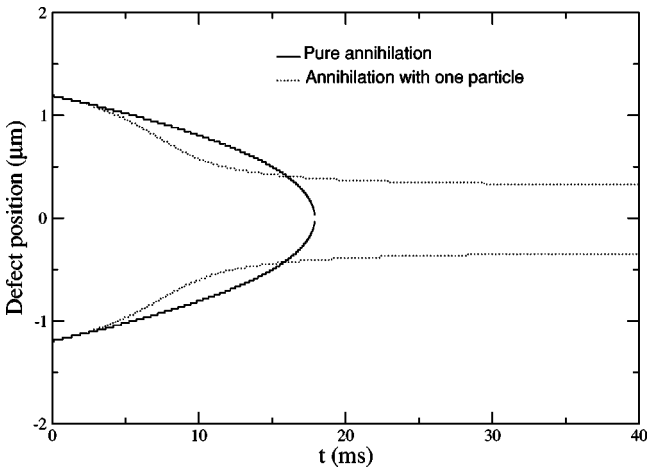

FIG. 8. Defect position during the annihilation of two disclination lines, in the presence of one particle, and in a ''pure'' annihilation process. (The lengths of the box are $L_x = L_y = 4.8$ μm.)

Figure 8 shows the defect positions of the two disclination lines. Let us recall that the defect positions are identified by looking for the minimum value of S. It is of interest to compare these results with those for a ''pure annihilation.'' The dynamic trajectories indicate that, in the presence of the particle, the disclination lines move faster than in the pure annihilation process. The increase in the velocity is significant for 5 ms$\leqslant t \leqslant$10 ms. This increase is induced by the two defects that are bound to the particle and that mediate an additive attractive force between the two lines. As mentioned previously, at $t \approx 12$ ms the three defects collapse, leading to a defect of topological charge $-1/2$. The minimum in the magnitude of S, from which the dynamic trajectories are defined, corresponds to the dynamic trajectory of the disclination line of charge $+1/2$ as long as $t \leqslant 12$ ms. But, after the collapse ($t \geqslant 12$ ms), the dynamic trajectory corresponds to the trajectory of the resulting $-1/2$ disclination line. As shown in Fig. 8, after the collapse of the three defects, we observe that the curvature of the dynamic trajectory changes. This indicates a decrease in the velocity of the defect. For $t \geqslant 12$ ms, the dynamic trajectory corresponds indeed to the relaxation of the $-1/2$ disclination lines towards their equilibrium location. The two disclination lines of charge $-1/2$ move in the direction of the surface of the particle until they reach an equilibrium position at a distance given by the ratio $a/R = 1.75$.

These two-dimensional simulations permit study of the effects of one particle on the dynamic behavior of disclination lines. However, a complete description of the director field requires simulation of a three-dimensional system. We have performed three-dimensional simulations to study the nematic order parameter and the structure of the director. Figure 9 illustrates the system considered in this work: two disclination lines are located along the y direction and are separated by a distance $d_z = 3.2$ μm. A particle with a radius $R = 0.2$ μm is located in the middle of the cell. This particular geometry was adopted because it mimics experiments currently underway in our laboratory. The simulations are performed on a grid of size $100 \times 100 \times 100$, and the lengths

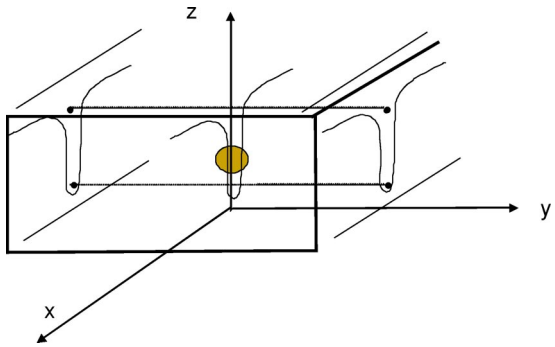

FIG. 9. Illustrative scheme representing the three-dimensional simulations: one spherical particle is located in the middle of the cell and two disclination lines are imposed in the y direction.

of the box are fixed at $L_x = L_y = L_z = 4$ μm. At the top and bottom surfaces, liquid crystal molecules are strongly anchored along the x direction. Periodic boundary conditions are imposed at the surfaces $y_{min} = -2$ μm and $y_{max} = 2$ μm.

Figure 10 represents the nematic order parameter in the yz plane, in the middle of the cell, and at three different time steps. The magnitude of S in this figure is represented by a color. The order parameter around the particle at $t = 0.05$ ms presents two minima in the equatorial plane. This indicates that, at the beginning of the simulation, the particle is surrounded by a Saturn Ring, parallel to the xy plane. This is also confirmed by the director configuration. The projection of the director configuration in the xy plane, in the middle of the cell, is represented in Fig. 11, at three different times. The observation of the Saturn ring in the initial moments of the calculations reflects that, at the beginning, and as long as the two disclination lines are far away from the particle, the director field in the neighborhood of the particle is quasiuniform with an average orientation of the molecules in the z direction (see Fig. 11 at $t = 8$ ms). As the two lines get closer to each other, they interact with the defect that accompanies the particle. In Fig. 10, it is observed that the lines are distorted near the particle (see the order parameter at $t = 14$ ms). Near the particle, the disclination lines are closer to each other, as compared to their locations at the extremities of the cell, at $y = \pm 2$ μm. This is in agreement with the results of two-dimensional simulations, showing that the presence of the particle increases the velocity of the disclination lines. The director configuration in the xz plane is similar to that obtained in two-dimensional simulations reported on the optical picture of Fig. 6; the Saturn ring is progressively distorted in such a way that the $+1/2$ disclination line attracts the $-1/2$ Saturn ring. From the director configuration shown in Fig. 11, one can see that at the surface of the particle the molecules are perpendicular to the surface and they progressively point in the z direction as one moves away from the center (see figure at $t = 8$ ms). As the disclination lines annihilate, the orientations of the molecules change in such a way that the molecules progressively rotate to be in the xy plane (see the figures at $t = 14$ ms and also at $t = 20$ ms). Finally, two defects of topological charge $-1/2$ are created near the particle (see the figure at $t = 20$ ms) and the final configuration corresponds to a particle surrounded

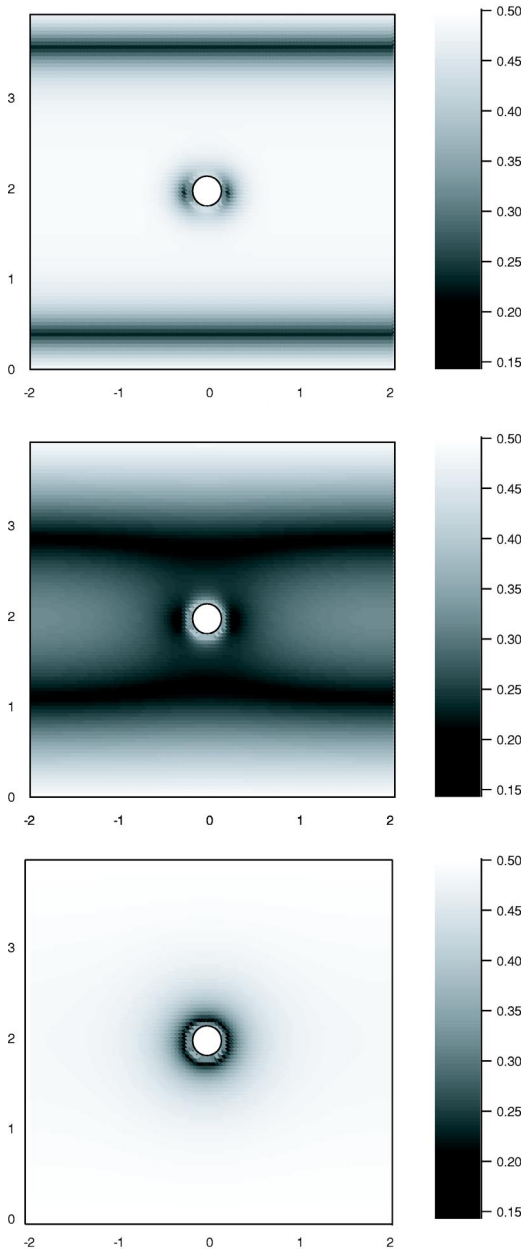

FIG. 10. Nematic scalar order parameter S in the yz plane. A color is attributed for the magnitude of S. From top to bottom, the snapshots are taken at $t=0.5$, 14, and 34 ms.

by a new Saturn ring in the yz plane. The final configuration with this new Saturn ring can also be clearly identified by the order parameter of Fig. 10, at time $t=34$ ms.

From the initial to the final configuration, the results of our simulations show that the location of the Saturn ring has pivoted around the particle, by an angle of $\pi/2$. These simulations suggest that experimentally the use of disclination lines could modify the defect structure of the particle: the use of disclination lines of opposite charges, which can be created through the application of an external field (for a magnitude of the field larger than the critical value of the Frederiks transition [21]), could permit control of the orientation of the Saturn ring around the particle.

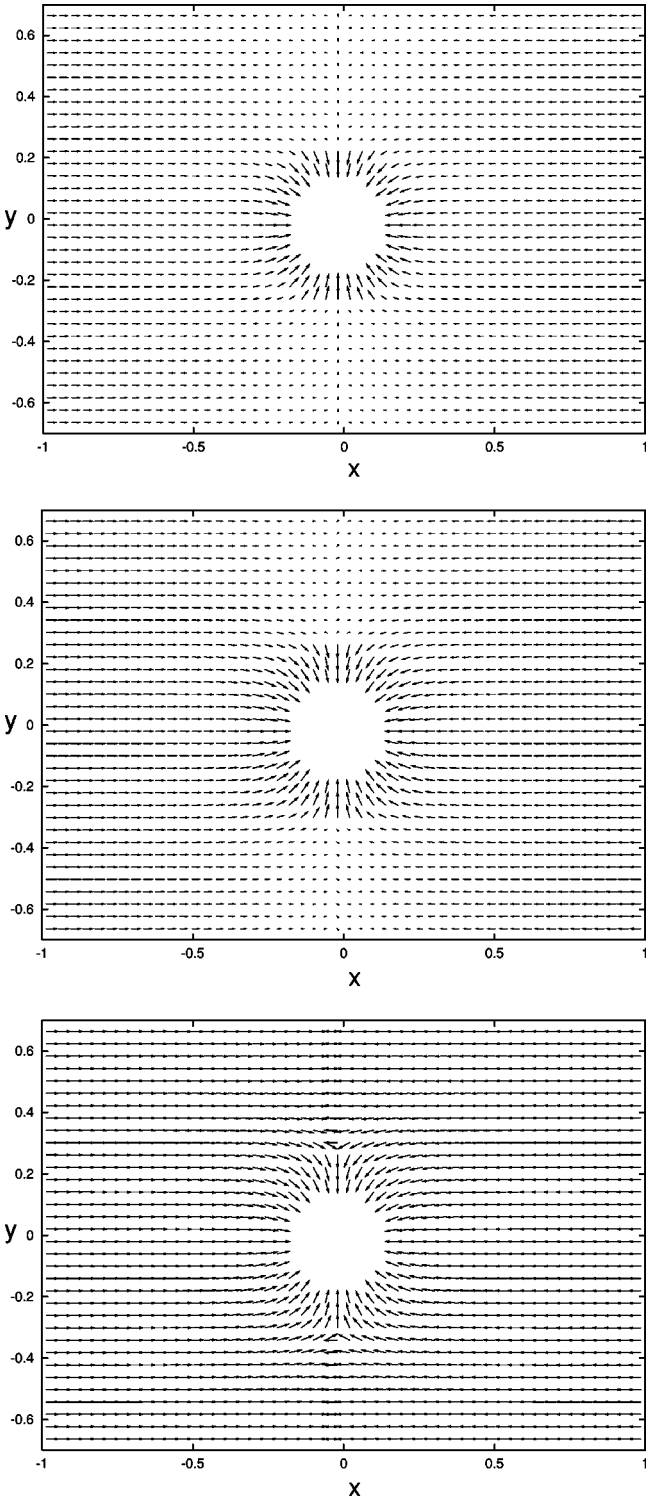

FIG. 11. Projection of the director configuration in the xy plane and near the particle: from top to bottom, the snapshots are taken at $t=8$, 14, and 20 ms.

IV. CONCLUSION

The dynamic behavior of a nematic liquid crystal has been examined within a tensor order parameter formalism. We have first considered the insertion of a single spherical

particle that anchors the molecules perpendicularly to its surface. The location of the defects that are bound to the particle has been analyzed for various sizes of the particle. It is found that a deviation from the continuum limit occurs when the radius of the particle R is smaller than the length scale ξ characteristic for changes in the nematic order parameter. For such submicrometer particles ($R \sim \xi$), the defects are repelled at a distance remote from the particle, and the linear expression giving the location of the defect for macroscopic particle is no longer valid. Using two- and three-dimensional simulations, we have examined the interaction between disclination lines and a particle. The results of these simulations suggest that a particle between two disclination lines could be surrounded by a Saturn ring. We find that the dynamics of the disclination lines are influenced by an effective interaction mediated by the topological defects that are bound to the particle. The two disclination lines feel a stronger attraction near the particle and are progressively distorted near the particle. As the two lines annihilate, they interact with the defect of the particle and the Saturn ring (around the particle) is progressively distorted. This process ends with a configuration where the particle is surrounded by a new Saturn ring. These results provide some insights on possible ways for controlling defect structure through the use of disclination lines, and will be the subject of a forthcoming experimental study.

ACKNOWLEDGMENT

This work was supported by the National Science Foundation through the University of Wisconsin's MRSEC on Nanostructured Interfaces.

[1] P. Poulin, V.A. Raghunathan, P. Richetti, and D. Roux, J. Phys. II **4**, 1557 (1994); P. Poulin, H. Stark, T.C. Lubensky, and D.A. Weitz, Science (Washington, DC, U.S.) **275**, 1770 (1997); P. Poulin and D.A. Weitz, Phys. Rev. E **57**, 626 (1998).

[2] J. Chen, P.J. Bos, H. Vithana, and D.L. Johnson, Appl. Phys. Lett. **67**, 2588 (1995).

[3] V.K. Gupta and N.L. Abbott, Science (Washington, DC, U.S.) **276**, 1533 (1997).

[4] Y. Gu and N.L. Abbott, Phys. Rev. Lett. **85**, 4719 (2000).

[5] V.K. Gupta, J.J. Skaife, T.B. Dubrovsky, and N.L. Abbott, Science (Washington, DC, U.S.) **279**, 2077 (1998).

[6] E.M. Terentjev, Phys. Rev. E **51**, 1330 (1995).

[7] O.V. Kuksenok, R.W. Ruhwandl, S.V. Shiyanovskii, and E.M. Terentjev, Phys. Rev. E **54**, 5198 (1996).

[8] O. Mondain-Monval, J.C. Dedieu, T. Gulik-Krzywicki, and P. Poulin, Eur. Phys. J. B **12**, 167 (1999).

[9] T.C. Lubensky, D. Pettey, N. Currier, and H. Stark, Phys. Rev. E **57**, 610 (1998).

[10] H. Stark, Eur. Phys. J. B **10**, 311 (1999).

[11] R.W. Ruhwandl and E.M. Terentjev, Phys. Rev. E **56**, 5561 (1997).

[12] S. Grollau, N. Abbott, and J.J. de Pablo, Phys. Rev. E (to be published).

[13] R.W. Ruhwandl and E.M. Terentjev, Phys. Rev. E **55**, 2958 (1997).

[14] B.I. Lev and P.M. Tomchuk, Phys. Rev. E **59**, 591 (1999).

[15] J.L. Billeter and R.A. Pelcovits, Phys. Rev. E **62**, 711 (2000).

[16] D. Andrienko, G. Germano, and M.P. Allen, Phys. Rev. E **63**, 041701 (2001).

[17] E.B. Kim, R. Faller, Q. Yan, N.L. Abbott, and J.J. de Pablo, J. Chem. Phys. **117**, 7781 (2002).

[18] N. Schopohl and T.J. Sluckin, Phys. Rev. Lett. **59**, 2582 (1987).

[19] Géza Tóth, Colin Denniston, and J.M. Yeomans, Phys. Rev. Lett. **88**, 105504 (2002).

[20] J. Fukuda and H. Yokoyama, Eur. Phys. J. E **4**, 389 (2001).

[21] P.G. de Gennes and J. Prost, *The Physics of Liquid Crystals*, 2nd ed. (Clarendon Press, Oxford, 1993).

[22] M. Doi and S.F. Edwards, *The Theory of Polymer Dynamics* (Clarendon Press, Oxford, 1989).

[23] A.N. Beris and B.J. Edwards, *Thermodynamics of Flowing Systems* (Oxford University Press, Oxford, 1994).

[24] Simulations were performed with $A=1$, $L_1=0.55$, $D^{\star}=0.35$, and $U=3$. These values imply $S^{eq}=0.5$, $\xi=1.81$, and $\Gamma=0.622$. Given suitable pressure, length, and time scales, these parameters can be mapped to $\xi=0.7\ \mu$m, $L_1=8.73$ pN, and $\Gamma=6.22\ \mathrm{Pa}^{-1}\,\mathrm{s}^{-1}$. The corresponding Frank elastic constants are then given by $K_11=K_22=K_33=4.37$ pN. These material parameters values are close to those of Ref. [19] and are representative of a 5CB liquid crystal.

[25] In two-dimensional simulations, the numerical resolutions are performed with various grids whose number of points varies from 160×160 to 500×500. We have used several time steps varying in the range $0.000\,01\leqslant\Delta t\leqslant0.001$. In three-dimensional simulations, we have used a grid $100\times100\times100$ and time steps varying in the range $0.001\leqslant\Delta t\leqslant0.004$.

[26] E.M. Terentjev, Phys. Rev. E **51**, 1330 (1995); O.V. Kuksenok, R.W. Ruhwandl, S.V. Shiyanovskii, and E.M. Terentjev, *ibid.* **54**, 5198 (1996); R.W. Ruhwandl and E.M. Terentjev, *ibid.* **56**, 5561 (1997).

[27] H. Stark, J. Stelzer, and R. Bernhard, Eur. Phys. J. B **10**, 515 (1999).